








Cite this: *Nanoscale*, 2020, **12**, 7735

Magnetically responsive layer-by-layer microcapsules can be retained in cells and under flow conditions to promote local drug release without triggering ROS production†

Jordan E. Read, ^a Dong Luo, ^b Tina T. Chowdhury, ^c Rod J. Flower,^a Robin N. Poston, ^d Gleb B. Sukhorukov ^{‡c} and David J. Gould ^{*‡a}

Nanoengineered vehicles have the potential to deliver cargo drugs directly to disease sites, but can potentially be cleared by immune system cells or lymphatic drainage. In this study we explore the use of magnetism to hold responsive particles at a delivery site, by incorporation of superparamagnetic iron oxide nanoparticles (SPIONs) into layer-by-layer (LbL) microcapsules. Microcapsules with SPIONs were rapidly phagocytosed by cells but did not trigger cellular ROS synthesis within 24 hours of delivery nor affect cell viability. In a non-directional cell migration assay, SPION containing microcapsules significantly inhibited movement of phagocytosing cells when placed in a magnetic field. Similarly, under flow conditions, a magnetic field retained SPION containing microcapsules at a physiologic wall shear stress of 0.751 dyne cm⁻². Even when the SPION content was reduced to 20%, the majority of microcapsules were still retained. Dexamethasone microcrystals were synthesised by solvent evaporation and underwent LbL encapsulation with inclusion of a SPION layer. Despite a lower iron to volume content of these structures compared to microcapsules, they were also retained under shear stress conditions and displayed prolonged release of active drug, beyond 30 hours, measured using a glucocorticoid sensitive reporter cell line generated in this study. Our observations suggest use of SPIONs for magnetic retention of LbL structures is both feasible and biocompatible and has potential application for improved local drug delivery.

Received 5th December 2019,
Accepted 7th February 2020

DOI: 10.1039/c9nr10329e

rsc.li/nanoscale

Introduction

Local treatment of disease is an important research goal because it can potentially increase efficacy of drugs whilst reducing side effects. To some extent this can be achieved by direct delivery of therapeutics into disease sites which also promotes local effects. However, with small molecule drugs and biologics, we know that they can be rapidly cleared from joints

and other sites *via* the blood stream and lymphatics.¹ An alternative is to use nano or micron sized particles as drug carriers from which prolonged release can be achieved. However, the persistence of vehicles at a desired site will depend on a range of criteria including cell phagocytosis and degradation, particle size, inflammation status of the site and lymphatic drainage. Work by Horisawa *et al.*, (2002) showed that nano-sized PLGA particles are readily phagocytosed by macrophages, whilst larger 26 µm particles remained extracellular in healthy rat joints.² When joints are inflamed, both nanosized (300 nm) vehicles and larger micronsized particles are removed by leakage and lymphatic drainage following intra-articular delivery.³

Glucocorticoids have potent anti-inflammatory and analgesic effects and are widely used in the treatment of rheumatoid and osteoarthritis patients by delivery directly to joints as micronized crystalline suspensions that slowly dissolve and have prolonged local effects.⁴ Nonetheless, following local delivery burst release results in elevation in blood levels of steroids⁵ which can cause systemic side effects.⁶ In addition

^aCentre for Biochemical Pharmacology, William Harvey Research Institute, Queen Mary University of London, London, EC1M 6BQ, UK.
E-mail: d.j.gould@qmul.ac.uk; Tel: +44 (0)2078823992

^bDepartment of Radiology, Case Western Reserve University, Cleveland, OH 44106, USA

^cInstitute of Bioengineering, School of Engineering and Materials Science, Queen Mary University of London, London, E1 4NS, UK

^dMicrovascular Research, William Harvey Research Institute, Queen Mary University of London, London, EC1M 6BQ, UK

†Electronic supplementary information (ESI) available. See DOI: 10.1039/c9nr10329e

‡These authors contributed equally.



there are reports of steroid crystals entering the lymphatics and causing hypopigmentation of covering skin^{7–9} and injections can cause a flare in disease which results from ingestion of crystals by phagocytic cells^{10,11} which can potentially migrate away from the delivery site.

There are now a number of nanomedicines that are approved for clinical use,¹² generally they aim to promote drug half-life or achieve a degree of passive targeting to disease sites. Future developments in nanomedicine will be active targeting to disease sites, triggered release in response to environmental or physical cues^{13,14} and theranostic capacity.¹⁵ We are interested nanoengineering delivery vehicles so that they are better retained at disease sites and to improve local treatment of disease. One nanoengineering approach, layer-by-layer (LbL) assembly first described by Decher *et al.* (1992)¹⁶ is a simple but flexible method to engineer nanoscale layers incorporating responsive particles and biological molecules into complex arrangements with functions ranging from sensors to drug delivery.^{17–19} LbL assembly applied to microparticles was first reported by Sukhorukov *et al.* (1998)²⁰ by the sequential addition of layers of alternatively charged polymers of approximately 2–3 nm in thickness²¹ on a template core. These microcapsules are ideally suited to the delivery of macromolecules that can be trapped within the structure of the capsule whereas small molecule drugs readily diffuse out unless they have affinity for a capsule component,²² layers are crosslinked to improve retention²³ or high drug loading is achieved by use of crystalline drug as the capsule core.²⁴ One of their interesting attributes is their potential for functionalisation through incorporation nanocomponents which can permit responsiveness to physical stimuli. Inclusion of superparamagnetic iron oxide nanoparticles (SPIONs) enables responsiveness to magnetism, which can be utilised to target vehicles²⁵ and control release of cargo molecules²⁶ through the use of permanent and alternating electromagnetic fields respectively. We know that microcapsules are readily phagocytosed by cells²⁷ and it is feasible that magnetism could be used to retain microcapsules at a delivered site and to prevent removal by cells or flow conditions. Indeed a recent report has shown magnetic retention of SPION containing microcapsules in the microvascular blood supply.²⁸ When SPIONs are used to provide magnetic responsiveness, there is however the concern that detrimental effects on cells will be caused by the production of reactive oxygen species (ROS).²⁹ Iron is known to catalyse the Fenton reaction that converts hydrogen peroxide, a product of lysosomes or mitochondrial oxidative respiration, into a highly toxic hydroxyl free radical (OH[•]). Despite this concern, in previous studies we have shown that SPION containing microcapsules are well tolerated by cells.²⁵ In this study we demonstrate that SPIONs incorporated into the microcapsule structure do not promote ROS production in cells. We also demonstrate that SPION containing microcapsules can be magnetically retained in a cell migration assay and under flow conditions. Furthermore, similar properties are seen with microcapsules formed from crystals of the glucocorticoid dexamethasone coated with polymer layers that incorporated SPIONs.

Experimental

Chemicals and reagents

All materials were supplied by Sigma-Aldrich unless otherwise stated.

Fabrication of empty LbL microcapsules

Empty LbL microcapsules (Empty-LbL) were constructed on a sacrificial calcium carbonate (CaCO₃) template using the LbL self-assembly technique (Fig. 1).³⁰ In brief, 2.5 ml of 0.33 M Calcium Chloride (CaCl₂) and 2.5 ml of 0.33 M Sodium Carbonate (Na₂CO₃) were combined in a beaker on a magnetic stirrer at 800 RPM for 30 seconds, 400 RPM for 30 seconds, then rested for 1 minute before centrifugation at 9000 RPM and collection. Poly L-Arginine (PLA) and Dextran Sulphate (DS) were used for biodegradable shells. All polymer solutions were used at 2 mg mL⁻¹ in 0.15 M Sodium Chloride (NaCl). Six alternative layers, *i.e.* three of each polymer, were assembled in total. PLA was assembled as the first layer by suspension of cores and shaking at room temperature for 12 minutes. Between polyelectrolyte layers, microcapsules were washed twice in deionised water. For fluorescent visualisation PLA-tetramethylrhodamine (PLA-TRITC) was added as the fifth polyelectrolyte layer. For magnetic microcapsules (Empty-LbL-Mag), SPIONs were synthesised as previously described³¹ then stabilised with citric acid and added in place of the fourth layer, followed by addition of DS to adsorb any remaining positive charge. For 100% SPION coverage stock nanoparticles in water of 45.8 µg mL⁻¹ was used and this suspension was further diluted 1:2 and 1:5 when used for reduced coverage.

Following multilayer assembly, the CaCO₃ cores were dissolved in ethylenediaminetetraacetic acid (EDTA) solution. Initially a 0.165 M solution of EDTA was added and microcapsules shaken for 7 minutes at room temperature. The concentration was increased to 0.2475 M and the shaking step repeated. Finally, three 0.33 M EDTA washes were conducted until cores were completely dissolved, when the microcapsules were washed in deionised water and stored at 4 °C until use. A summary of the structure of Empty-LbL and Empty-LbL-Mag microcapsules is given in Table 1.

Fabrication of dexamethasone containing LbL microcapsules

Dexamethasone crystals were produced by dissolution of dexamethasone powder in acetone at a concentration of 10 mg mL⁻¹. 500 µL of dexamethasone–acetone solution was added to 2 mL of 2% Tween-80 in H₂O and was sonicated using a Piezon Master 400 dental sonication probe for 3 minutes at maximum power. Dexamethasone solution was stir evaporated at room temperature for 30 minutes, which formed crystals which were collected *via* centrifugation at 9000 RPM for 2 minutes and then washed twice with deionised water. LbL encapsulation of dexamethasone crystals (Dex-LbL) was carried out immediately. Poly(allylamine hydrochloride) (PAH) and poly(styrenesulfonate) (PSS) were used for synthetic shells. These polymer solutions were again prepared at 2 mg mL⁻¹ in



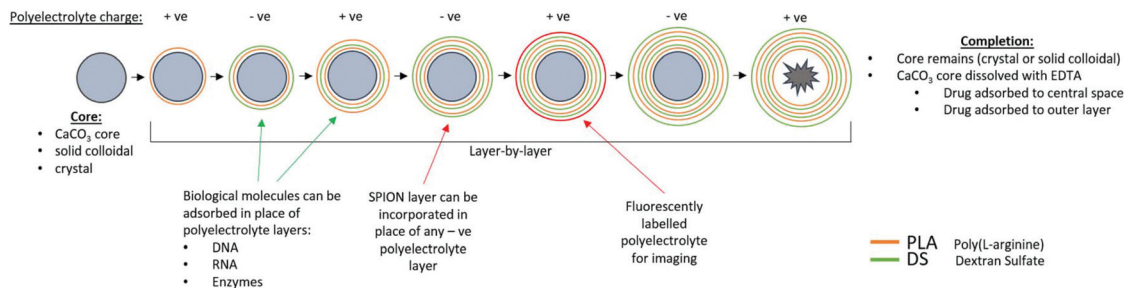


Fig. 1 Production of polyelectrolyte layer-by-layer microcapsules. Shown is an overview of the production of LbL microcapsules. The process begins with a core, upon which oppositely charged polyelectrolyte layers are added. The process ends with dissolution of the core (if sacrificial). Cargo molecules can be encapsulated in the core, adsorbed in place of polyelectrolyte layers, or adsorbed to the microcapsule following core dissolution. A fluorescently labelled polyelectrolyte layer can be added for visualisation and a SPION layer can be added in place of a negatively charged polyelectrolyte layer. The number of layers, polyelectrolytes used and biological molecule content can all be altered to tailor LbL microcapsules to the desired specifications.

Table 1 Structure of LbL microcapsules produced in this study. Shown are the four types of microcapsules constructed and the order of polyelectrolyte layers applied in their production

Microcapsule	Composition of polyelectrolyte layers
Empty-LbL	Sacrificial CaCO ₃ core/PLA/DS/PLA/DS/PLA-TRITC/DS
Empty-LbL-Mag (100%/50%/20%)	Sacrificial CaCO ₃ core/PLA/DS/PLA/SPION/PLA-TRITC/DS
Dex-LbL	Dex crystal/PAH/PSS/PAH/PSS/PAH/PSS/PAH-TRITC/PSS
Dex-LbL-Mag	Dex crystal/PAH/PSS/PAH/SPION/PAH/PSS/PAH-TRITC/PSS

0.15 M NaCl. Eight polymer layers were assembled in total, with PAH assembled as the first layer. For magnetic dexamethasone microcapsules (Dex-LbL-Mag), SPIONs were added in place of the fourth layer followed by addition of PSS to neutralise any remaining positive charge. A summary of the structure of Dex-LbL and Dex-LbL-Mag microcapsules is given in Table 1.

Percentage encapsulation of dexamethasone was calculated by application of layer washes to 293T.GRE.Luc+ cells at a dilution of 1:100 in Dulbecco's Modified Eagle Medium (DMEM) cell culture media. For confirmation of stable polymer layers, 20 μ L of Dex-LbL microcapsules were spun onto a glass slide, by centrifugation at 2000 RPM for 3 minutes. Dex-LbL crystals were viewed under phase contrast and red fluorescence to image the drug crystal and PAH-TRITC polyelectrolyte layer respectively, and images were overlaid. A 10 μ L drop of acetonitrile was added to the structures to dissolve the dexamethasone and the field of view immediately imaged again (Fig. S1†).

For all other steroid crystals, alterations were made to the crystallisation method. For dissolution of prednisolone and prednisolone acetate, chloroform:methanol (1:1) was used as the solvent. Methylprednisolone acetate was dissolved in acetone. Prednisolone crystals were then produced by the above sonication method. Prednisolone acetate and methylprednisolone acetate crystals required a homogenisation

method, in which 1 mL of steroid solution was added to 5 mL of 2% Tween-80 in H₂O and was homogenised using an IKA Ultra Turrax T8 Homogenizer (Janke & Kunkel GmbH & Co. KG) for 3 minutes at speed setting 4. Stir evaporation was carried out as above and crystals were stored at 4 °C until use.

Scanning electron microscopy

Microcapsule and crystal appearance was assessed by imaging using an FEI Inspect-F scanning electron microscope (SEM). Following production, microcapsule samples were suspended in 1 ml of deionised water before further dilution 1:10 in deionised water. Three small drops were distributed on carbon tape upon a metal stump and were allowed to dry completely. For acetonitrile dissolution of LbL dexamethasone crystals, 10 μ L of acetonitrile was subsequently added to stumps and allowed to evaporate completely (Fig. S1†). Before imaging, samples were sputter coated with gold using a Quorum SC7620 sputter coater for 30 seconds. Coated samples were imaged using the FEI inspect-F SEM with FEI xT microscope control software, at varying magnifications up to 20 000 \times .

Generation of the enhanced green fluorescent protein (EGFP) expressing HeLa cell line

For visualisation of cell movement, a HeLa cell line, stably expressing EGFP was generated by transduction of HeLa cells (ATCC® CCL-2™) with the EGFP encoding lentiviral construct pHRIS-CSGW-dlNotI (kindly provided by Dr Y. Ikeda, Mayo Clinic, Rochester, MN). To produce lentivirus, 6.16 μ g of pHRIS-CSGW-dlNotI construct was packaged *via* co-transfection with, 1.5 μ g pCMV-VSV-G, 6.13 μ g pCMV- Δ 8.2 and 68 μ g polyethylenimine (PEI), into HEK 293T cells (ATCC® CRL-3216™) seeded at 1 million per well in a 6-well plate. Cell growth media was changed 5 hours post-transfection and cells grown for 48 hours, before harvesting of virus containing media. Media was applied to HeLa cells seeded at 10 000 per well in a 6-well plate, with addition of 6 μ g mL⁻¹ polybrene to the virus containing media. Cells were grown and monitored for 48 hours, before transfer into a T25 tissue culture flask. HeLa-EGFP cells were subjected to FACS sorting, to isolate and



subculture the 25% brightest EGFP expressing cells for use in experiments.

Generation of the glucocorticoid responsive 293T.GRE.Luc⁺ cell line

Oligonucleotides were designed that harbour the glucocorticoid responsive element (GRE, in bold), the sequence of the forward primer was 5' CTAGCACCTCACGGTACATTTTGTCTGTGCCTCG 3' and the reverse primer was 5' CTAGCGAGGCAC-AGAACAAATGTACCGTGAGGTG 3'. These phosphorylated oligonucleotides were annealed and repeats cloned between the Nhe I and Xho I sites of the previously described plasmid pCpGmCMVLuc⁺.³² Sequence analysis confirmed the construction of a synthetic promoter consisting of 4 repeats of the GRE upstream from the mCMV promoter. The expression cassette was then transferred to the lentiviral vector LV.mCMV.Luc⁺³² by PCR cloning, forming the vector pLV.GRE.Luc⁺. Lentivirus was generated using the method described above and virus containing media was applied to HEK 293T cells seeded at 10 000 per well in a 6-well plate, with addition of 6 µg ml⁻¹ polybrene to the virus containing media. Cells were grown and monitored for 48 hours before transferring into a T25 tissue culture flask. 293T.GRE.Luc⁺ cells were tested for steroid responsiveness, using dilutions of dexamethasone. Glucocorticoid responsiveness was monitored by measurement of luciferase production. Cells were maintained in complete media (Dulbecco's Modified Eagle medium (DMEM, Gibco) supplemented with 10% fetal calf serum (Gibco) 1% penicillin-streptomycin and 1% L-glutamine). Cells were passaged 1:10, using trypsin EDTA, once a confluence of 100% was reached and were used within 5 passages.

Confocal microscopy

To assess cell uptake of Empty-LbL-Mag microcapsules, HeLa cells were plated on coverslips at a density of 10 000 per well in a 6-well plate. 24 hours post plating, TRITC labelled Empty-LbL-Mag microcapsules were added to the cells at a ratio of 10:1. Cells were incubated for 30 minutes, 1 hour and 2 hours. Cells were stained post treatment by washing twice in ice cold PBS and subsequent addition of a 1× dilution of CellMaskTM Green Plasma Membrane Stain (ThermoFisher Scientific) in cell culture media, for 10 minutes. To fix cells, staining media was removed and 4% paraformaldehyde was applied for 20 minutes at room temperature. Cells were washed twice in PBS before mounting, using VECTASHIELD[®] mounting media with 4',6-diamidino-2-phenylindole (DAPI, Vector Laboratories, Peterborough, UK). Cells were immediately imaged using an LSM 880 confocal microscope with Airyscan (Zeiss Microscopy, Cambridge, UK) and Zen 2.3 software (Zeiss), using the DAPI, 488 nm and 568 nm laser channels and a 40× objective. All image analysis and processing was carried out using Zen 2.3 Lite software (Zeiss).

Cell migration assay

HeLa-EGFP cells were seeded at a density of 20 000 cells per well in 6-well plates in a central circle, defined using parafilm

cut with a 6 mm biopsy punch. On the underside of the well a grid was drawn with fluorescent marker, as shown in Fig. 3A. After 6 hours incubation at 37 °C cells had attached and media was replaced with fresh complete media. Microcapsules were applied at a 1:1 ratio to the plated cells and incubated for 24 hours. At time point 0 hours the parafilm was removed, cells washed twice with complete media and fresh 2 ml of media applied to each well. Circular 5 mm diameter × 5 mm thick N42 Neodymium Magnets (Magnet Expert Ltd, Nottinghamshire, UK) were used, which had maximum field strength of 191 mT as measured with a HT201 gaussmeter (EMF, UK). Magnets were applied to the underside of relevant wells directly below the circle of cells and remained in place for the duration of the experiment, aside from imaging. Areas of interest adjoining to the central circle (Fig. 3A) were imaged at 0, 96, 120, 144 and 168 hours using an EVOSTM digital colour fluorescence microscope (Thermo Fisher Scientific UK) in the four defined areas of interest, under the DAPI and EGFP fluorescence channels.

The DAPI and EGFP images were overlaid into a composite image. Image analysis was performed with a macro written in Image Pro software. Thresholds were set for the EGFP colour channel so that the cells but not the background were detected. No measurements were carried out with the DAPI as it was used only for the purpose of lining up the images on the microscope for imaging. For EGFP, the area of interest was selected as the whole field of view and the data recorded for the % area filled with EGFP, corresponding to the area filled with cells.

ROS assay

293T.GRE.Luc⁺ and HeLa cells plated at a density of 20 000 cells in 96-well plates were treated for 2 hours or 24 hours with defined numbers of microcapsules or equivalent concentrations of SPIONs, diluted in DMEM supplemented with 5% FCS, 1% pen-strep and 1% L-glutamine, before ROS assays were carried out. Treatments were removed and cells washed once with warmed DMEM. 100 µL of dichloro-dihydro-fluorescein diacetate (DCFH-DA, Sigma-Aldrich), diluted in serum free DMEM to a concentration of 10 µM was added to wells and incubated in the dark at 37 °C for 30 minutes. Plate fluorescence was read at excitation/emission 485 nm/535 nm using a Tecan GENios microplate reader (Tecan Group Ltd, Männedorf, Switzerland). For additional stimulation of ROS, 100 µL of 0.01% hydrogen peroxide, diluted in DMEM media was added following removal of media. Cells were incubated at 37 °C for 1 hour, before washing and detection of ROS with DCFH-DA.

Cell viability

In parallel with the ROS experiments, cells that were similarly treated with microcapsules or SPIONs were assessed for cell viability after 24 hours of treatment. In these experiments the CellTiter-Glo[®] (Promega Corp) assay was performed by addition of 100 µl titreGLO assay reagent to each well. Plates were briefly shaken and then incubated for 20 minutes before



the luminescent signal in 1 second was recorded using a plate luminometer.

Ferene-S iron assays

Ferene-S assay was carried out using the method described by Hedayati *et al.*, (2018).³³ Iron standards between 0 and 100 μg were produced using the TraceCERT® Iron Standard for ICP. Defined numbers of microcapsules or SPIONs, suspended in 100 μL PBS were dissolved by mixing with 100 μL concentrated nitric acid and incubated for 2 hours at 80 $^{\circ}\text{C}$. Acid was neutralised by addition of 160 μL 10 N sodium hydroxide. Ferene-S Assay working solution was prepared, composition 0.2 M L-ascorbic acid, 0.4 M acetate buffer, 0.1 M Ferene-S. 900 μL of Ferene-S Assay working solution was added to 100 μL of iron standard, microcapsule or nanoparticle sample and incubated at room temperature for 30 minutes. Absorbance of 300 μL of samples was read in triplicate in a 96-well plate, at 595 nm, using a MultiSkan FC (Thermo Fisher Scientific UK). Iron concentrations were determined using the standard curve and nanoparticle and microcapsule iron content calculated.

Flow system investigations

As a model for therapeutic microcapsules immobilised by a magnet, a flow system was assembled using an Econo-Column® peristaltic pump (Bio-Rad Laboratories Ltd, Hertfordshire, UK). Initial collections of volumes of deionised H_2O over a period of 1 minute at each flow speed were conducted to determine flow rate in $\mu\text{L min}^{-1}$. The terminal length of plastic tubing was applied across a 0.9 kg pull rectangular $10 \times 3.5 \times 2.25$ mm thick N45 neodymium magnet with a maximum field strength of 182.5 mT at the poles. To test retention of magnetic microcapsules, 5 million microcapsules were applied to the flow system by reverse pumping at low speed until they reached the magnet. Flow was reverted to the forward direction and the slowest pump speed selected. After 5 minutes at each flow speed, photographs were taken and the retention of the microcapsules assessed by densitometry analysis of the photographs, using ImageJ (<https://imagej.nih.gov/ij/index.html>).

Measurement of dexamethasone release from magnetically retained microcapsules

10 million LbL-Dex or LbL-Dex-mag microcapsules were applied to the flow system by reverse pumping at low speed until they reached the magnet. Flow was reverted to the forward direction at flow speed 5 ($0.385 \text{ dyne cm}^{-2}$). Flow through of deionised water containing released dexamethasone was collected every 20 minutes for 10 hours then at 24, 30 and 48 hours. At termination of the experiment the magnet was removed from the tubing and the remaining deionised water in the system collected, with any remaining microcapsules. To assay dexamethasone, 293T.GRE.Luc+ cells were plated at a seeding density of 20 000 cells per well in a 96 well plate. Samples from the flow experiment were applied to cells in triplicate at a 1 : 5 dilution in DMEM supplemented with 5% FCS, 1% pen-strep and 1%

L-glutamine. 24 hours post-treatment cells were lysed with passive lysis buffer (50 μL). A luciferase assay was performed on lysates (10 μL) in white plastic 96-well plates to which 50 μL of assay reagent was automatically added using an MLX Microtiter® Plate Luminometer (Dynex Technologies Inc., Chantilly, VA, USA) and light emission measured for 10 seconds. Dexamethasone standard concentrations were applied to the cells to produce a standard curve.

Statistical methods

Statistical analysis of results was carried out using GraphPad Prism 7.04 (GraphPad Software, La Jolla California, USA). For analysis of flow retention experiments, results were subjected to 2-way ANOVA analysis with multiple comparisons and *post-hoc* Bonferroni test. For cell retention experiments, results were subjected to 2-way ANOVA analysis with multiple comparisons (simple effect within rows) and *post-hoc* Turkey test. ROS assay data was subjected to one-way ANOVA with multiple comparisons and Fisher's LSD *post-hoc* test.

Results and discussion

LbL microcapsules have many features that make them suited to application in drug delivery.^{34,35} They can be assembled from FDA approved polymers under native conditions which are compatible with a range of bioactive molecules from DNA and proteins through to small molecule drugs. Beyond this, microcapsules can be loaded with particles that provide responsiveness to physical signals such as gold nanoparticles for NIR laser heating³⁶ and SPIONs for magnetic responsiveness. We are particularly interested in magnetic responsiveness as we have previously shown targeted delivery²⁵ and controlled release through this attribute.²⁶ In the present study, we have turned our attention to magnetic retention which could be important when microcapsules are delivered to a disease site and the aim is to prevent their removal in order to promote local drug effects.

Microcapsule appearance and cell uptake

Empty non-magnetic (Empty-LbL) and magnetic microcapsules (Empty-LbL-Mag) were characterised using SEM, fluorescent and confocal microscopy. Microcapsules were measured as $2.57 \pm 0.10 \mu\text{m}$ in diameter (Fig. 2A). The SPION layer was visible as a roughened surface in Empty-LbL-Mag. Both types of microcapsule were of similar size and resemble those reported in previous studies made by the LbL sacrificial calcium carbonate core method.^{25,37} Fluorescence microscopy confirmed a TRITC labelled PLA layer, with a hollow microcapsule core (Fig. 2B), which enabled confocal microscopy visualisation of microcapsule interaction with HeLa cells. Time-course incubation of SPION containing microcapsules with HeLa cells demonstrated interaction after just 30 minutes, maintained through 2 hours of co-incubation (Fig. 2C). In addition, Z-stack confocal scanning indicated that after 1 hour of incubation, microcapsules were inside the cells. Many of the microcapsules were adjacent to the nucleus which again is



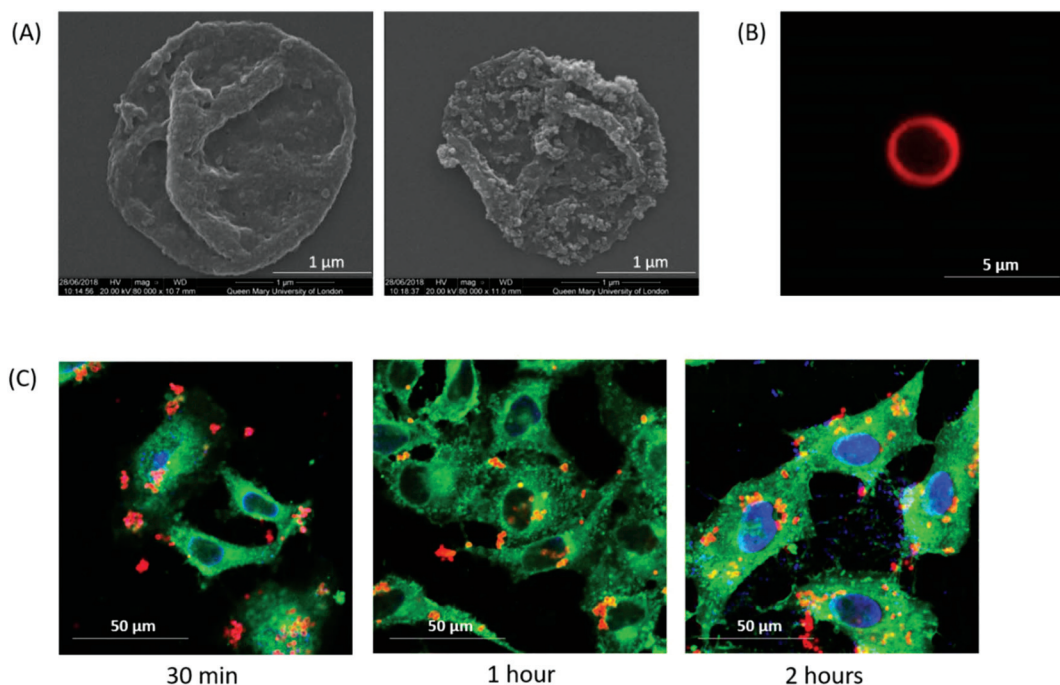


Fig. 2 Image analysis of layer-by-layer microcapsules. (A) representative SEM images of a control empty core LbL microcapsule (Empty-LbL) (left) and an LbL microcapsule with SPION layer (Empty-LbL-Mag) (right) magnification 80 000x. (B) Representative fluorescent image of the PLA-TRITC layer of a control Empty-LbL microcapsule. (C) Time course confocal microscopy of interaction of Empty-LbL-Mag microcapsules (red) with HeLa cells (green) and their DAPI stained nuclei (blue).

consistent with previous observations of standard microcapsules in other cells.³⁸ Importantly, there are no obvious differences in the appearance of cells, microcapsule uptake rate or intracellular trafficking when the magnetic version are delivered.

Controlling SPION content of microcapsules correlates with measurement of iron content

To date, studies utilising magnetic microcapsules have typically used an excess of SPIONs to produce one or more complete iron oxide shells.^{25,39,40} Here, to establish more stringent control over the iron content of the microcapsules, empty core magnetic microcapsules were made with varying percentage coverage of SPIONs in the fourth layer. Visual analysis of microcapsules assembled with 100%, 50% and 20% SPION suspension clearly demonstrated that as the nanoparticle content was reduced, the roughened surface appearance of the microcapsules was reduced accordingly (Fig. 3A). Using the Ferene-S assay (standard curve Fig. 3B) the iron content of microcapsules with 100% SPION coverage was measured to be 20.2 pg per microcapsule (Fig. 3C). Dilution of SPION suspension 1 : 2 produced microcapsules with a lower iron content of 12.28 pg per microcapsule (Fig. 3C), about 60% of the iron content of the microcapsules prepared with the 100% suspension. A further dilution of the SPIONs to 1 in 5 produced microcapsules with an iron content of 4.11 pg per microcapsule, and 20.3% of the iron content of the microcapsules pre-

pared with the 100% suspension (Fig. 3C). The ability to alter SPION content could ensure the minimum iron content to achieve a desired functional effect, whilst increasing microcapsule biocompatibility could potentially permit delivery of higher microcapsule doses or facilitate repeat delivery. Our data would suggest that there is further scope to reduce SPION content of microcapsules whilst retaining magnetic responsiveness. What the precise lower limit of SPION content is will largely depend on the magnetic function that is required.

Biocompatibility of microcapsules containing SPIONs and their influence on ROS production

Iron is a catalyst of free radical production including the toxic OH^\bullet from H_2O_2 which can cause cell death. In view of this, there are concerns that iron nanoparticles can lead to ROS production. We have previously observed that SPION containing microcapsules do not alter cell viability except when they are at high ratios to cells and after prolonged exposure.²⁵ Here we saw that SPION containing microcapsules did not alter the viability of HeLa or 293T cells after 24 hours of exposure (Fig. 3D) and furthermore there was no induction of ROS regardless of the iron content of microcapsules, compared to control untreated cells (Fig. 3E). Similarly, delivery of free magnetite nanoparticles, equivalent to the content in microcapsules, also had no effect on cell viability (Fig. 2D) or ROS production (Fig. 3E). Our observations are in agreement with other researchers. Könczöl *et al.*, (2011)⁴¹ showed that A549 cells exposed to a similar concentration ($10 \mu\text{g ml}^{-1}$) of slightly



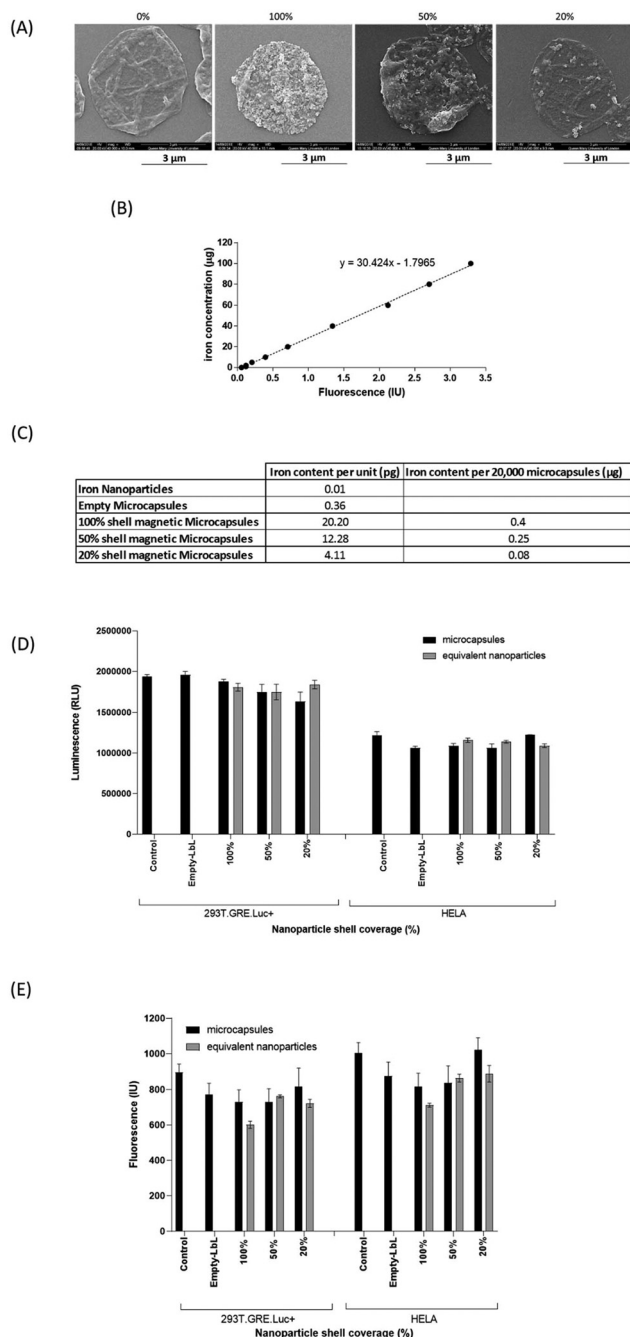


Fig. 3 Production of reactive oxygen species in response to SPION containing microcapsules. (A) Appearance of Empty-LbL-Mag microcapsules made with dilutions of SPION suspensions, using Scanning Electron Microscopy. (B) Ferene-S iron assay standard curve used to determine iron content of microcapsules. (C) Table showing the iron content of SPION containing Empty-LbL-Mag microcapsules in terms pg iron per microcapsule, content in 20 000 microcapsules as added to experimental wells for a 1:1 ratio of microcapsules: cells, and as a $\mu\text{g mL}^{-1}$ concentration. (D) Viability of 293T.GRE.Luc+ cells or HeLa cells treated with a 1:1 ratio of Empty-LbL-Mag microcapsules: cells, or the equivalent number of free SPIONS for 24 hours as determined using CellTiter viability assay. (E) Production of ROS in 293T.GRE.Luc+ cells or HeLa cells treated with a 1:1 ratio of Empty-LbL-Mag microcapsules: cells, or the equivalent number of free SPIONS for 24 hours. As a control Empty-LbL microcapsules with no SPIONS were added at 1:1 ratio of microcapsules: cells. $N = 3$. Standard error of the mean in bar charts is shown by the vertical lines.

larger (20–60 nm) magnetite nanoparticles for 24 hours had ROS levels comparable to control cells. Whilst, Aranda *et al.* (2013)⁴² incubated smaller magnetite nanoparticles (8 nm) with primary rat hepatocytes and saw no increase in ROS production until cells were exposed to an Fe_3O_4 concentration of $50 \mu\text{g mL}^{-1}$ for 24 hours. Although our results clearly show that the levels of ROS produced by cells after delivery of microcapsules containing SPIONS are not elevated it has been reported that similar citrate coated small magnetite nanoparticles can induce a transient increase in cellular stress which was evident by an increase of malonyldialdehyde (an indicator of lipid peroxidation) immediately after delivery to a macrophage cell line.⁴³ We examined ROS production 2 hours after delivery of microcapsules or nanoparticles to cells but again there was no change in this parameter from untreated cells (Fig. S2†). Concentration of iron is clearly an important factor. The observations on cellular stress made by Stroh used magnetite in excess of $300 \mu\text{g mL}^{-1}$ and the effects observed on ROS production seen by Aranda followed use of $50 \mu\text{g mL}^{-1}$ whereas the concentration delivered in our microcapsule study equates to a maximum of $4 \mu\text{g mL}^{-1}$. Further work exploring the kinetics of cell utilisation of the iron delivered in microcapsules will be useful when repeat delivery is considered in order to avoid accumulation of iron to levels that alter cell function and viability.

Another possibility to be considered is that SPIONS will exacerbate hydroxyl radical (OH^\bullet) synthesis if they are delivered into an environment containing H_2O_2 . If we consider the use of SPION containing microcapsules in treatment of inflammatory conditions this is important because H_2O_2 released from activated polymorphonuclear leucocytes can be present in the inflammatory milieu. ESI (Fig. S3A†) shows that hydrogen peroxide treatment (1 hour) of cells causes a dose dependent increase in ROS production. When cells were pre-treated (24 hours) with free SPIONS or SPION containing microcapsules before exposure to a suboptimal concentration of H_2O_2 (0.01%) for an hour there was no further exacerbation of ROS production (Fig. S3B†). These observations are encouraging for the *in vivo* use of SPION containing microcapsules in inflammatory environments.

Retention of cells following delivery of SPION containing microcapsules

Magnetic microcapsules may be of use in maintaining encapsulated drugs in their desired area of action within the body. One issue to overcome is the possibility that phagocytic cells may engulf microcapsules and remove them from the site of action. To this end, cell retention studies were carried out to determine whether the iron content of the Empty-LbL-Mag microcapsules was sufficient to prevent cell movement in a magnetic field. In this assay a magnet was placed directly beneath the cells which generated the magnetic field (strength maximum of 200 mT in the centre) illustrated in Fig. S4†. Images were collected at set time points after the start of the experiment (Fig. 4A and B) and these were used to determine the movement of HeLa-EGFP cells into adjacent areas of inter-



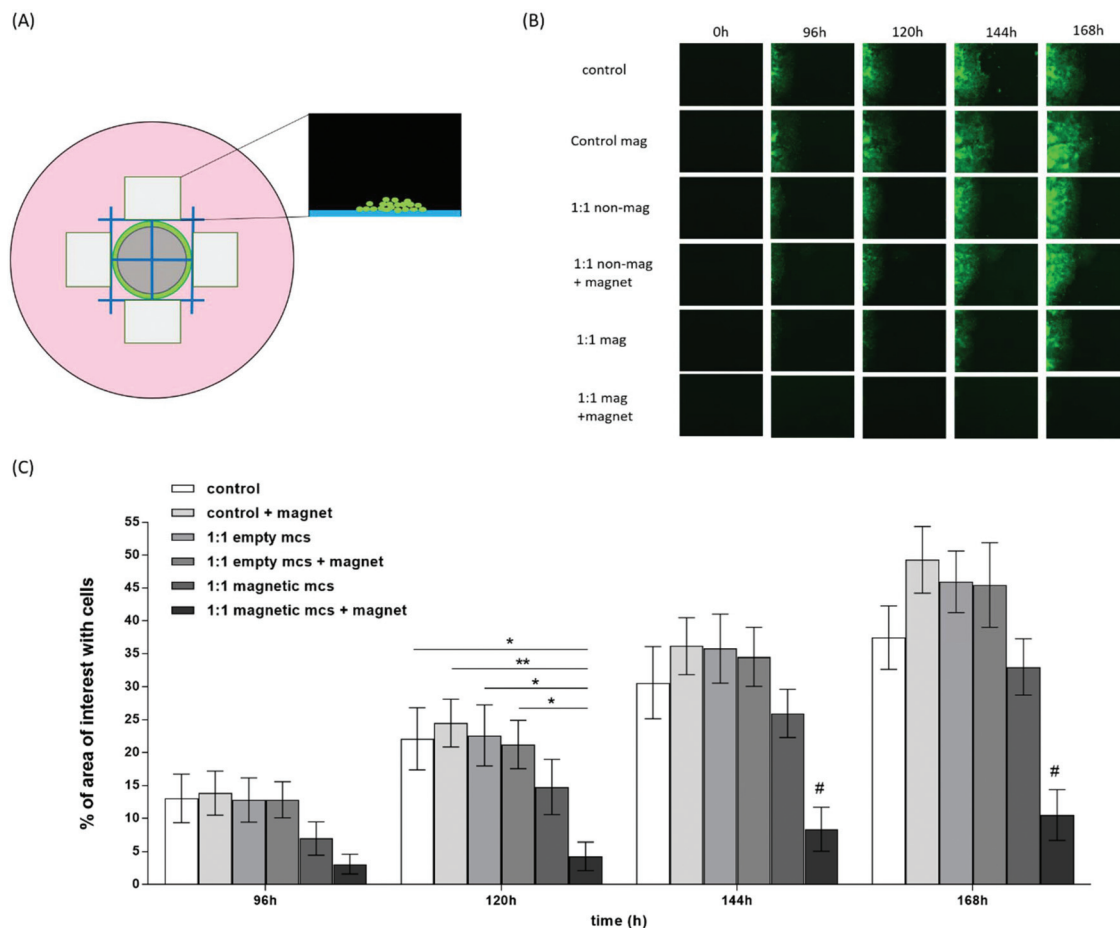


Fig. 4 Retention of HeLa-EGFP cells treated with SPION containing microcapsules (Empty-LbL-Mag) in a magnetic field. (A) Schematic of experimental set up. Green circle represents area of plated HeLa-EGFP cells, grey circle represents 5 mm neodymium magnet, blue lines represent reference grid and the rectangles represent the four areas of interest imaged, one border of which is adjacent to the area of plating as shown. The magnified region shows a representation of an imaged area of interest, with migrated cells. (B) HeLa-EGFP cell images taken in a single area of interest over the time course of a single experiment. (C) Movement of HeLa-EGFP cells treated with control Empty-LbL microcapsules (Empty mcs) or SPION containing Empty-LbL-Mag microcapsules (Magnetic mcs (100% SPION shell)) into the area of interest, under control conditions or when subjected to a magnetic field from a N42 neodymium magnet. Area of interest values are the mean of four separate areas of interest and error bars represent standard error of the mean. Cell movement into the areas of interest was measured at intervals up to 168 hours. Significant differences are indicated by * $p < 0.05$, ** $p < 0.01$. # $p < 0.05$ relative to all other treatments at the same timepoint. Data is representative of two experimental repeats.

est by image analysis. HeLa-EGFP cells containing Empty-LbL-Mag microcapsules at a 1:1 ratio of microcapsules to cells, moved significantly less than control cells at all time points beyond 96 hours when they were placed in a magnetic field. At 120 hours cells preincubated with Empty-LbL-Mag microcapsules in a magnetic field (Fig. 4B and C: 1:1 mag + magnet) had filled 4.29% of the area of interest, demonstrating significantly less movement than control cells (22.12%, $p = 0.0316$), control cells in a magnetic field (control mag, 24.49%, $p = 0.009$), cells + Empty-LbL (1:1 non-mag, 22.63%, $p = 0.0244$) and cells + Empty-LbL microcapsules in a magnetic field (1:1 non-mag + magnet, 21.26%, $p = 0.0477$). At 144 hours, cells preincubated with Empty-LbL-Mag microcapsules and exposed to a magnetic field had filled 8.38% of the area of interest, significantly less than all other cell treat-

ments ($p = 0.035$). This observation was maintained through to 168 hours, where cells with Empty-LbL-Mag microcapsules in a magnetic field had filled only 10.53% of the region of interest ($p = 0.0023$); significantly less compared to all other cell treatments (Fig. 4C). The observations in this experiment are important for several reasons; firstly, because they further support the idea that SPION containing microcapsules are inert in cells, because in the absence of a magnetic field they did not significantly alter cell migration in this assay, even at the longest timepoint. When cells containing SPION containing microcapsules (Empty-LbL-Mag) were placed in a fixed magnetic field, the distance they migrated was dramatically inhibited. This inhibition was solely due to the interaction of the SPION containing microcapsules with the magnetic field, as movement of HeLa cells containing standard microcapsules



(Empty-LbL) was not inhibited. These results are encouraging and suggest that it may be possible to retain microcapsules engulfed by cells at a delivered site *in vivo* if similar interaction with a magnetic field can be recapitulated.

Retention of microcapsules with different SPION contents in a flow system

Application of SPION containing Empty-LbL-Mag microcapsules to a flow system demonstrated that even microcapsules prepared with a 20% SPION suspension were retained at shear stresses between 0.046–0.751 dyne cm^{-2} (corresponding to flow speeds between 0.1–1.64 ml min^{-1} in a 1.5 mm diameter tube) (Fig. 5). Densitometry analysis of microcapsule pellets retained on a fixed magnet demonstrated that as the shear stress increased, there was no loss in retention of the 100% SPION shell microcapsules until the highest stress of 0.751 dyne cm^{-2} was reached (Fig. 5B), where a 10% reduction was observed. For the microcapsules prepared with 50% and 20% SPION suspensions retention was reduced to 90% and 85% respectively by a shear stress of 0.385 dyne cm^{-2} and was further reduced to 80% retention for both shell contents at the highest shear stress (Fig. 5). These observations with a flow system (shear rates of 0.046–0.751 dyne cm^{-2}) show that SPION containing microcapsules could potentially be magnetically retained in the type of flow and shear stress conditions observed in lymphatic vessels (2 μl per hour⁴⁴ to 30 $\mu\text{l min}^{-1}$ ⁴⁵) and have average shear stress of 0.64 dyne cm^{-2} .⁴⁶ Although flow rates increase during inflammation to reduce oedema and facilitate removal of cells.⁴⁷ Based on our findings, retention may also be possible in small veins (diameters from 800 μm to 1.8 mm) where flow rates of 1.2–4.8 ml min^{-1} have been measured, corresponding to shear stresses of between 0.028–3.435 dyne cm^{-2} .⁴⁸

Generation of steroid crystals coated with LbL assemblies

Multiple steroids are used in the treatment of inflammatory conditions; hence we used four steroids for formulation into solvent evaporation steroid crystals. Dexamethasone crystals had a homogenous appearance and were approximately $9.22 \pm 0.68 \mu\text{m}$ in size, with a rounded, flattened cuboidal shape of depth $1.49 \pm 0.11 \mu\text{m}$ (Fig. 6A). Prednisolone crystals had less homogeneity, with crystals mostly hexagonal in shape and with an average size of $4.32 \pm 0.42 \mu\text{m}$, depth $0.82 \pm 0.12 \mu\text{m}$. Prednisolone acetate formulated as crystals gave a homogenous suspension of triangular shape crystals, with an average size of $5.44 \pm 0.13 \mu\text{m}$ and depth $0.29 \pm 0.04 \mu\text{m}$. Methylprednisolone crystals were long and octagonal in shape with an average length of $8.89 \pm 0.43 \mu\text{m}$, width of $2.71 \pm 0.16 \mu\text{m}$ and depth of $0.37 \pm 0.03 \mu\text{m}$ (Fig. 6A). In comparison to crystalline steroid preparations currently used clinically to treat inflammation in arthritic joints, such as Depo-Medrol[®], our crystals were more homogenous in size and shape, have a smoother surface and are of similar size.⁴⁹

To confirm stable polymer layers, LbL encapsulated dexamethasone crystals were imaged using fluorescence microscopy and scanning electron microscopy, before and after dissolution with acetonitrile (ESI Fig. S1†). Prior to dissolution the dexamethasone crystals and fluorescent polyelectrolyte layer were both clearly visible (Fig. S1A–C†). After dissolution with acetonitrile, the dexamethasone crystals were no longer visible, but the fluorescent polyelectrolyte layer was still visible and intact, confirming that the polyelectrolyte layers formed a stable structure around the steroid crystal (Fig. S1D–F†). SEM imaging was used to confirm these findings, also showing that following acetonitrile dissolution, the polyelectrolyte shells remained visible and retained the crystal shape, whilst the solid crystal was no longer visible (Fig. S1G and H†).

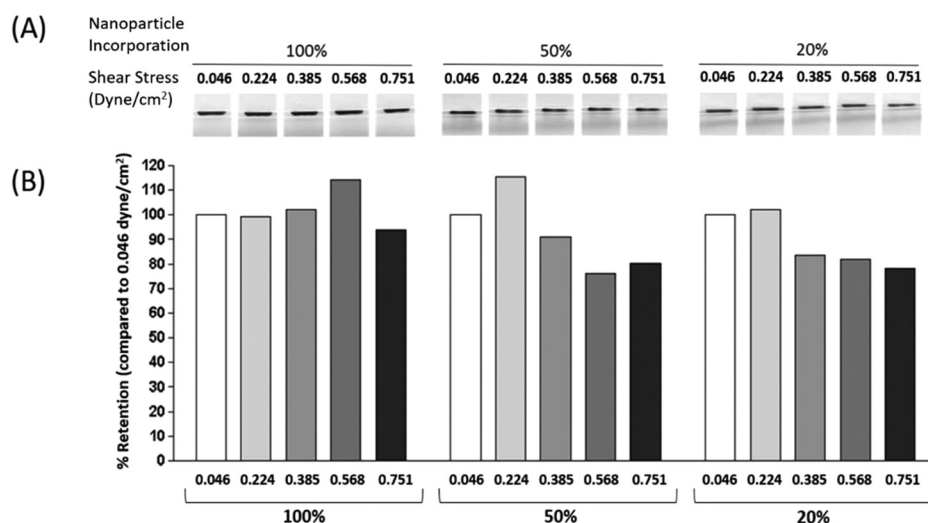


Fig. 5 Retention of magnetic microcapsules in a flow system. (A) Images of retained Empty-LbL-Mag microcapsules in 1.5 mm diameter tubing, taken using a fixed position camera following 5 minutes at each flow speed. In the absence of microcapsules no band was seen, and (B) quantified % retention of Empty-LbL-Mag microcapsules in a flow system at increasing shear stresses for 5 minutes per condition (expressed as a % of retention compared to the value at the lowest shear stress of 0.046 dyne cm^{-2}).



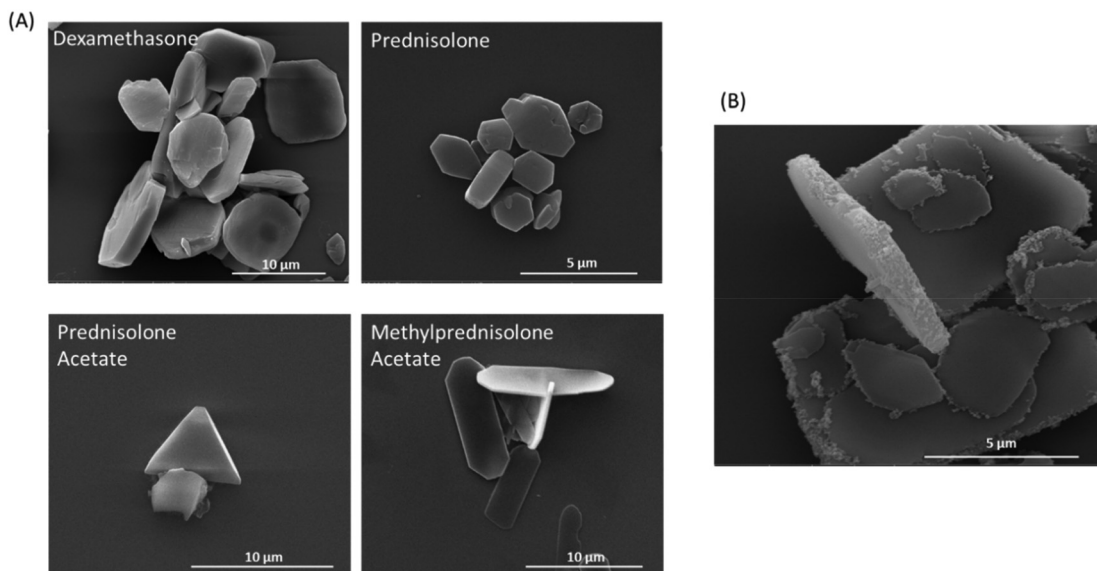


Fig. 6 Crystals of different corticosteroids. (A) SEM images of different corticosteroid crystals made by the oil-in-water emulsion technique. (B) SEM of LbL encapsulated dexamethasone crystals with a SPION layer (Dex-LbL-Mag).

The LbL method used within this paper is well characterised and has been used many times before on both colloidal sacrificial cores and crystalline cores.^{24,25}

When a layer of SPIONs was included in the coating of dexamethasone crystals (Dex-LbL-Mag), they were a largely homogenous suspension of flattened cuboidal crystals of size $9.22 \pm 0.68 \mu\text{m}$, with slightly rounded square sides and with a dexamethasone encapsulation efficiency calculated to be up to 99.99%. The iron content was measured to be approximately 5.03 pg per microcapsule and the distribution of SPIONs was largely on the narrow edge of the crystals as shown (Fig. 6B). The reason for this distribution around the narrow edge of the crystals may be because this surface has an increased charge, due to its curvature and rough layer growth at the edge, in comparison to the flat face of the crystals, therefore the SPIONs attach more readily on this surface. Alternatively, the SPIONs may attach to the planar crystal surfaces but many are mechanically sheared off when the planar surfaces slide across each other in the shaking stages of the encapsulation process.

Responsiveness of 293T.GRE.Luc+ cells

In order to monitor dexamethasone release from fabricated microcapsules, the glucocorticoid responsive cell line, 293T.GRE.Luc+ was used. Treatment of the 293T.GRE.Luc+ cell line with dexamethasone standard concentrations between 0.1 nM and 10 μM demonstrated that the cells were sensitive between 1 nM and 10 μM, as shown by a near-linear dose response (Fig. 7A). Treatment of 293T.GRE.Luc+ cells with a 1 : 1 ratio of un-encapsulated dexamethasone crystals, Dex-LbL and Dex-LbL-Mag demonstrated dexamethasone release from all structures, resulting in significant luciferase production compared to untreated cells after 24 hours. Luciferase production was increased 109.2-fold over control levels in cells treated with

Dex crystals (7624.3 ± 440.8 vs. 69.8 ± 1.3 , $p < 0.0001$). Dex-LbL microcapsules drove luciferase production 129.3-fold over control levels (9024.1 ± 759.9 $p < 0.0001$) and Dex-LbL-Mag microcapsules drove luciferase production 102.5-fold over control levels (7154.0 ± 693.4 , $p < 0.0001$) (Fig. 7B). Biological activity was also shown for all the different steroid crystals by treatment of GC responsive 293T cells (data not shown). Most studies that monitor steroid release from vehicles use HPLC or UV-Vis absorbance to quantitate steroid release. HPLC has a reported limit of quantification around 10 nM^{50,51} and UV/Vis has a lower detection limit of around 1 μM.^{52,53} The reporter cell line we generated utilising an optimally designed promoter for low basal activity and robust activation³² enabled us to accurately measure dexamethasone concentrations in the range 1 nM to 10 μM. In addition to improved sensitivity, the reporter cells also have the advantage that it confirms biological activity of the drug. This type of transcriptionally responsive system is particularly useful in monitoring drug released from nano/micro fabricated vehicles and can be combined with imaging modalities to monitor positional effects of released drug.²⁵

When we coated our dexamethasone crystals with polymer layers their appearance was not altered and they released similar amounts of dexamethasone as uncoated crystals. When dexamethasone has previously been coated in LbL layers, irregular micronized crystals of the drug have been used.^{54,55} Pargaonkar *et al.*, (2005)⁵⁴ sonicated crystals in the presence of poly(diallyldimethylammonium chloride) (PDPA) to form nanosized crystals (mean diameter 420 nm) which they coated in different polymer layers, whilst Stewart *et al.*⁵⁵ generated LbL structures similar in size (7.40 μm) to the ones we constructed. In both studies rapid release (100% within 120 minutes) of dexamethasone from LbL structures was



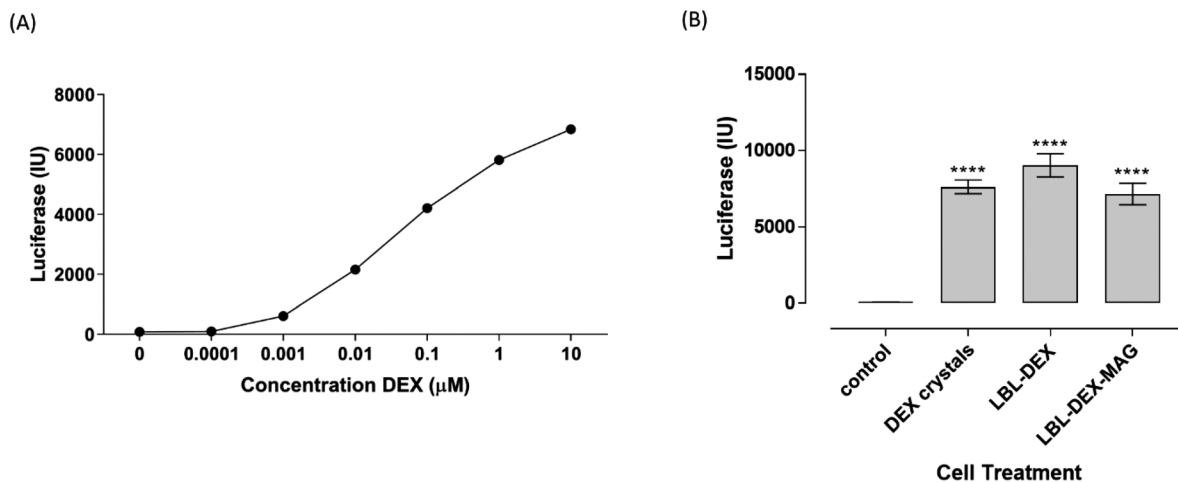


Fig. 7 Dexamethasone response of 293T.GRE.Luc+: (A) luciferase response of 293T.GRE.Luc+ cells to standard concentrations of dexamethasone solution after 24 hours. (B) Luciferase response of 293T.GRE.Luc+ cells to dexamethasone crystal constructs applied at a 1:1 ratio of crystals to cells after 24 hours. Each value is the mean of triplicate readings and error bars are standard error of the mean; **** represents a significant difference of $p < 0.0001$ compared to control cell response.

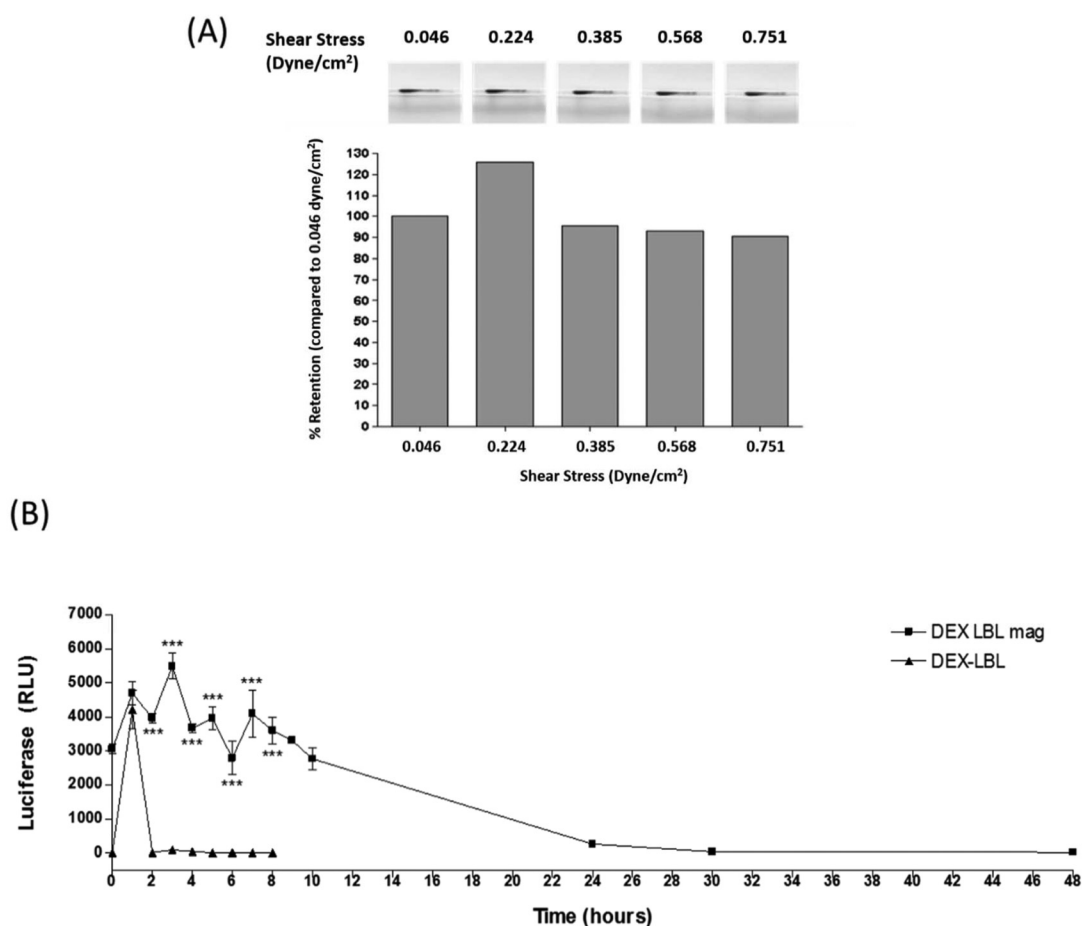


Fig. 8 Retention of magnetic LbL encapsulated dexamethasone crystals in a flow system. (A) Images of retained dexamethasone crystals in a flow tube, which are quantified in the bar chart below. Dexamethasone crystals in a flow system when subjected to increasing shear stress for 5 minutes at each shear stress rate (expressed as a % of retention at lowest shear stress of 0.046 dyne cm^{-2}). (B) Luciferase response of 293T-GRE-Luc+ cells to dexamethasone released into deionised water from non-magnetic dexamethasone crystals (Dex-LbL) or SPION containing LbL dexamethasone crystals (Dex-LbL-Mag) retained in the tubing with a permanent magnet over a period of 24 hours. *** $p < 0.001$ (compared to time matched Dex-LbL).



Table 2 A summary of the findings of this study. Microcapsule properties of Empty-LbL-Mag and Dex-LbL-Mag microcapsules are shown

Microcapsule property	Empty-LbL-magnetic microcapsules	Magnetic LbL dexamethasone crystals
Iron content (pg per microcapsule)	100% shell = 20.20 pg per microcapsule 50% shell = 12.28 pg per microcapsule 20% shell = 4.11 pg per microcapsule	5.03 pg per microcapsule Comparable to 20% shell
Internalised by cells	Rapidly internalised (for 100%)	Not tested
Cell viability	No effect on cell viability at 1 : 1 ratio	Not tested
ROS production in live cells	No ROS production for any	Not tested
Cells retainable in magnetic field	Yes	Not tested
Retainable under flow conditions $0.751 \text{ dyne cm}^{-2}$	Yes, at least 80% (for all)	Yes (80%)

observed, but Pargaonkar *et al.* (2005)⁵⁴ observed a slower rate of release with increasing number of microcapsule polymer layers. Prednisolone crystals have also been incorporated into LbL structures⁵⁶ and again slower release was observed when coated with more polymer layers.

Prolonged release of Dex from crystals magnetically retained in a flow system

In order to determine whether prolonged dexamethasone release in a flow system was possible, densitometry analysis was carried out on pellets of SPION containing Dex-LbL-Mag microcapsules applied to a fixed magnet in the flow system of increasing shear stress. Retention of Dex-LbL-Mag at the lowest stress of $0.046 \text{ dyne cm}^{-2}$ was 100%, reducing to 95.36% at $0.385 \text{ dyne cm}^{-2}$ and further reducing to 90.57% at the highest stress of $0.751 \text{ dyne cm}^{-2}$ (Fig. 8A). Long term retention studies carried out at the lowest shear stress of $0.046 \text{ dyne cm}^{-2}$ over a 48 hours period demonstrated that dexamethasone was removed from the flow system after 4 hours of application when non-magnetic Dex-LbL microcapsules were applied to the fixed magnet (Fig. 8B). Application of SPION containing Dex-LbL-Mag microcapsules demonstrated a significantly longer release of dexamethasone over a period of 48 hours. Quantification of dexamethasone in the flow through was significantly higher for Dex-LbL-Mag at 2 hours post application, with luciferase response measuring $3962.7 \pm 150.0 \text{ RLU}$ compared to $7.79 \pm 3.60 \text{ RLU}$ for Dex-LbL ($p < 0.001$). The concentration of dexamethasone in the flow through remained significantly higher for Dex-LbL-Mag ($3600.13 \pm 399.60 \text{ RLU Luc}$) compared to baseline values for Dex-LbL until 8 hours post application ($p < 0.001$). Beyond this time point, samples for Dex-LbL were not collected. Between 8 hours and 48 hours the concentration of dexamethasone in the flow through from Dex-LbL-Mag microcapsules steadily declined but even after 48 hours the dexamethasone level was above 5 nM. Furthermore, the remaining water collected from the flow system after 48 hours also contained measurable dexamethasone so the Dex-LbL-Mag microcapsules were still not exhausted at the end of this experiment. Clearly these studies show that magnetically retained Dex-LbL-Mag microcapsules result in prolonged release of dexamethasone under shear stress conditions beyond 30 hours. Whilst this compares favourably to the rapid release seen from dexamethasone LbL structures in other reports^{54,55} direct comparison is not possible due to differences

in the protocols of the release experiments. Taken together the data suggests that these dexamethasone microcapsules could potentially be magnetically retained at a delivered site, achieve prolonged drug action and resist removal by flow forces either in the lymphatics or small blood vessels.

Conclusions

Our experiments show that SPION containing microcapsules do not cause cellular stress following delivery and they can be magnetically retained at sites under both physiologically relevant shear stress conditions and following cell engulfment. A summary of the main findings of this study can be found in Table 2. If we can demonstrate the same characteristics *in vivo* we should be able to retain vehicles at delivery sites in order to promote local drug effects. We show how this approach can be utilised with magnetically responsive dexamethasone crystals and anticipate that it could be explored with other drug cargoes.

Conflicts of interest

The authors have no competing interests.

Acknowledgements

The authors thank Mr Russell Bailey of Nanovision (QMUL) for help with SEM and Dr Oliver Haworth for FACS sorting the HeLa-EGFP cells. This work was supported by *Versus Arthritis* [grant number 21210] and Dong Luo was funded by the China Scholarship Council.

References

- 1 S. G. Owen, H. W. Francis and M. S. Roberts, Disappearance kinetics of solutes from synovial fluid after intra-articular injection, *Br. J. Clin. Pharmacol.*, 1994, **38**(4), 349–355.
- 2 E. Horisawa, K. Kubota, I. Tuboi, K. Sato, H. Yamamoto, H. Takeuchi, *et al.*, Size-dependency of DL-lactide/glycolide copolymer particulates for intra-articular delivery system



- on phagocytosis in rat synovium, *Pharm. Res.*, 2002, **19**(2), 132–139.
- 3 J. Pradal, P. Maudens, C. Gabay, C. A. Seemayer, O. Jordan and E. Allémann, Effect of particle size on the biodistribution of nano- and microparticles following intra-articular injection in mice, *Int. J. Pharm.*, 2016, **498**(1), 119–129.
 - 4 N. Gerwin, C. Hops and A. Lucke, Intraarticular drug delivery in osteoarthritis, *Adv. Drug Delivery Rev.*, 2006, **58**(2), 226–242.
 - 5 R. D. Armstrong, J. English, T. Gibson, J. Chakraborty and V. Marks, Serum methylprednisolone levels following intra-articular injection of methylprednisolone acetate, *Ann. Rheum. Dis.*, 1981, **40**(6), 571–574.
 - 6 A. Stout, J. Friedly and C. J. Standaert, Systemic Absorption and Side Effects of Locally Injected Glucocorticoids, *PM R*, 2019, **11**(4), 409–419.
 - 7 P. C. McCormack, G. N. Ledesma and J. G. Vaillant, Linear Hypopigmentation After Intra-articular Corticosteroid Injection, *Arch. Dermatol.*, 1984, **120**(6), 708–709.
 - 8 C. Schwartz, S. Javvaji and J. S. Feinberg, Linear rays of hypopigmentation following intra-articular corticosteroid injection for post-traumatic degenerative joint disease, *Dermatol. Online J.*, 2012, **18**(5), Retrieved from <https://escholarship.org/uc/item/13d68647>.
 - 9 A. Gupta, M. Garg, N. Johnson and P. Vignesh, Hypopigmentation after intra-articular corticosteroid injection, *BMJ Case Rep.*, 2019, **12**(3), e228921.
 - 10 R. G. Berger and W. J. Yount, Immediate “steroid flare” from intraarticular triamcinolone hexacetonide injection: Case report and review of the literature, *Arthritis Rheum.*, 1990, **33**(8), 1284–1286.
 - 11 D. White and S. Munroe, Clinical image: crystal arthritis induced by intraarticular corticosteroid, *Arthritis Rheum.*, 2011, **63**(8), 2539.
 - 12 C. L. Ventola, Progress in Nanomedicine: Approved and Investigational Nanodrugs, *P T*, 2017, **42**(12), 742–755.
 - 13 Y. Liang, X. Zhao, P. X. Ma, B. Guo, Y. Du and X. Han, pH-responsive injectable hydrogels with mucosal adhesiveness based on chitosan-grafted-dihydrocaffeic acid and oxidized pullulan for localized drug delivery, *J. Colloid Interface Sci.*, 2019, **536**, 224–234.
 - 14 M. Mackiewicz, J. Romanski, K. Drabczyk, E. Waleka, Z. Stojek and M. Karbarz, Degradable, thermo-, pH- and redox-sensitive hydrogel microcapsules for burst and sustained release of drugs, *Int. J. Pharm.*, 2019, **569**, 118589.
 - 15 A. Sneider, D. VanDyke, S. Paliwal and P. Rai, Remotely Triggered Nano-Theranostics For Cancer Applications, *Nanotheranostics*, 2017, **1**(1), 1–22.
 - 16 G. Decher, J. D. Hong and J. Schmitt, Buildup of ultrathin multilayer films by a self-assembly process: III. Consecutively alternating adsorption of anionic and cationic polyelectrolytes on charged surfaces, *Thin Solid Films*, 1992, **210–211**(Part 2(0)), 831–835.
 - 17 A. C. Soares, J. C. Soares, F. M. Shimizu, V. D. C. Rodrigues, I. T. Awan, M. E. Melendez, *et al.*, A simple architecture with self-assembled monolayers to build immunosensors for detecting the pancreatic cancer biomarker CA19–9, *Analyst*, 2018, **143**(14), 3302–3308.
 - 18 X. Zhang, Y. Xu, X. Zhang, H. Wu, J. Shen, R. Chen, *et al.*, Progress on the layer-by-layer assembly of multilayered polymer composites: Strategy, structural control and applications, *Prog. Polym. Sci.*, 2019, **89**, 76–107.
 - 19 K. Ariga, E. Ahn, M. Park and B. S. Kim, Layer-by-Layer Assembly: Recent Progress from Layered Assemblies to Layered Nanoarchitectonics, *Chem.-Asian J.*, 2019, **14**(15), 2553–2566.
 - 20 G. Sukhorukov, E. Donath, S. Davis, H. Lichtenfeld, F. Caruso, V. Popov, *et al.*, Step-Wise Polyelectrolyte Assembly on Particle Surfaces – A Novel Approach to Colloid Design, *Polym. Adv. Technol.*, 1998, **9**, 759–767.
 - 21 E. Donath, G. B. Sukhorukov, F. Caruso, S. A. Davis and H. Mohwald, Novel Hollow Polymer Shells by Colloid-Templated Assembly of Polyelectrolytes, *Angew. Chem., Int. Ed.*, 1998, **37**(16), 2201–2205.
 - 22 D. Luo, D. J. Gould and G. B. Sukhorukov, Local and Sustained Activity of Doxycycline Delivered with Layer-by-Layer Microcapsules, *Biomacromolecules*, 2016, **17**(4), 1466–1476.
 - 23 C. A. Ghiorghita, F. Bucatariu and E. S. Dragan, Influence of cross-linking in loading/release applications of polyelectrolyte multilayer assemblies, A review, *Mater. Sci. Eng., C*, 2019, **105**, 110050.
 - 24 D. Luo, S. Shahid, R. M. Wilson, M. J. Cattell and G. B. Sukhorukov, Novel Formulation of Chlorhexidine Spheres and Sustained Release with Multilayered Encapsulation, *ACS Appl. Mater. Interfaces*, 2016, **8**(20), 12652–12660.
 - 25 A. M. Pavlov, S. A. Gabriel, G. B. Sukhorukov and D. J. Gould, Improved and targeted delivery of bioactive molecules to cells with magnetic layer-by-layer assembled microcapsules, *Nanoscale*, 2015, **7**(21), 9686–9693.
 - 26 D. Luo, R. N. Poston, D. J. Gould and G. B. Sukhorukov, Magnetically targetable microcapsules display subtle changes in permeability and drug release in response to a biologically compatible low frequency alternating magnetic field, *Mater. Sci. Eng., C*, 2019, **94**, 647–655.
 - 27 L. Kastl, D. Sasse, V. Wulf, R. Hartmann, J. Mircheski, C. Ranke, *et al.*, Multiple internalization pathways of polyelectrolyte multilayer capsules into mammalian cells, *ACS Nano*, 2013, **7**(8), 6605–6618.
 - 28 D. V. Voronin, O. A. Sindeeva, M. A. Kurochkin, O. Mayorova, I. V. Fedosov, O. Semyachkina-Glushkovskaya, *et al.*, In Vitro and in Vivo Visualization and Trapping of Fluorescent Magnetic Microcapsules in a Bloodstream, *ACS Appl. Mater. Interfaces*, 2017, **9**(8), 6885–6893.
 - 29 J. Paunovic, D. Vucevic, T. Radosavljevic, S. Mandić-Rajčević and I. Pantic, Iron-based nanoparticles and their potential toxicity: Focus on oxidative stress and apoptosis, *Chem.-Biol. Interact.*, 2020, **316**, 108935.
 - 30 A. M. Pavlov, G. B. Sukhorukov and D. J. Gould, Location of molecules in layer-by-layer assembled microcapsules influences activity, cell delivery and susceptibility to enzyme degradation, *J. Controlled Release*, 2013, **172**(1), 22–29.



- 31 R. Sheparovych, Y. Sahoo, M. Motornov, S. Wang, H. Luo, P. N. Prasad, *et al.*, Polyelectrolyte Stabilized Nanowires from Fe₃O₄ Nanoparticles via Magnetic Field Induced Self-Assembly, *Chem. Mater.*, 2006, **18**(3), 591–593.
- 32 H. Mohamed, Y. Chernajovsky and D. Gould, Assembly PCR synthesis of optimally designed, compact, multi-responsive promoters suited to gene therapy application, *Sci. Rep.*, 2016, **6**, 29388.
- 33 M. Hedayati, B. Abubaker-Sharif, M. Khattab, A. Razavi, I. Mohammed, A. Nejad, *et al.*, An optimised spectrophotometric assay for convenient and accurate quantitation of intracellular iron from iron oxide nanoparticles, *Int. J. Hyperthermia*, 2018, **34**(4), 373–381.
- 34 W. Tong, X. Song and C. Gao, Layer-by-layer assembly of microcapsules and their biomedical applications, *Chem. Soc. Rev.*, 2012, **41**(18), 6103–6124.
- 35 A. S. Timin, D. J. Gould and G. B. Sukhorukov, Multi-layer microcapsules: fresh insights and new applications, *Expert Opin. Drug Delivery*, 2017, 1–5.
- 36 A. M. Pavlov, A. V. Sapelkin, X. Huang, K. M. P'Ng, A. J. Bushby, G. B. Sukhorukov, *et al.*, Neuron cells uptake of polymeric microcapsules and subsequent intracellular release, *Macromol. Biosci.*, 2011, **11**(6), 848–854.
- 37 L. I. Kazakova, L. I. Shabarchina, S. Anastasova, A. M. Pavlov, P. Vadgama, A. G. Skirtach, *et al.*, Chemosensors and biosensors based on polyelectrolyte microcapsules containing fluorescent dyes and enzymes, *Anal. Bioanal. Chem.*, 2013, **405**(5), 1559–1568.
- 38 A. Muñoz Javier, O. Kreft, M. Semmling, S. Kempter, A. G. Skirtach, O. T. Bruns, *et al.*, Uptake of Colloidal Polyelectrolyte-Coated Particles and Polyelectrolyte Multilayer Capsules by Living Cells, *Adv. Mater.*, 2008, **20**(22), 4281–4287.
- 39 W. Zhang, L. Deng, G. Wang, X. Guo, Q. Li, J. Zhang, *et al.*, Low-Magnetization Magnetic Microcapsules: A Synergistic Theranostic Platform for Remote Cancer Cells Therapy and Imaging, *Part. Part. Syst. Charact.*, 2014, **31**(9), 985–993.
- 40 S. Carregal-Romero, P. Guardia, X. Yu, R. Hartmann, T. Pellegrino and W. J. Parak, Magnetically triggered release of molecular cargo from iron oxide nanoparticle loaded microcapsules, *Nanoscale*, 2015, **7**(2), 570–576.
- 41 M. Könczöl, S. Ebeling, E. Goldenberg, F. Treude, R. Gminski, R. Gieré, *et al.*, Cytotoxicity and Genotoxicity of Size-Fractionated Iron Oxide (Magnetite) in A549 Human Lung Epithelial Cells: Role of ROS, JNK, and NF-κB, *Chem. Res. Toxicol.*, 2011, **24**(9), 1460–1475.
- 42 A. Aranda, L. Sequeda, L. Tolosa, G. Quintas, E. Burello, J. V. Castell, *et al.*, Dichloro-dihydro-fluorescein diacetate (DCFH-DA) assay: a quantitative method for oxidative stress assessment of nanoparticle-treated cells, *Toxicol. in Vitro*, 2013, **27**(2), 954–963.
- 43 A. Stroh, C. Zimmer, C. Gutzeit, M. Jakstadt, F. Marschinke, T. Jung, *et al.*, Iron oxide particles for molecular magnetic resonance imaging cause transient oxidative stress in rat macrophages, *Free Radicals Biol. Med.*, 2004, **36**(8), 976–984.
- 44 C. Blatter, E. F. J. Meijer, A. S. Nam, D. Jones, B. E. Bouma, T. P. Padera, *et al.*, In vivo label-free measurement of lymph flow velocity and volumetric flow rates using Doppler optical coherence tomography, *Sci. Rep.*, 2016, **6**, 29035.
- 45 N. McHale, Nervous Control of the Lymphatic System, *Vasc. Med. Rev.*, 1993, **vmr-4**(4), 307–319.
- 46 J. B. Dixon, S. T. Greiner, A. A. Gashev, G. L. Cote, J. E. Moore Jr. and D. C. Zawieja, Lymph Flow, Shear Stress, and Lymphocyte Velocity in Rat Mesenteric Prenodal Lymphatics, *Microcirculation*, 2006, **13**(7), 597–610.
- 47 Z. Yuan, H. Rodela, J. B. Hay, D. Oreopoulos and M. G. Johnston, Lymph flow and lymphatic drainage of inflammatory cells from the peritoneal cavity in a casein-peritonitis model in sheep, *Lymphology*, 1994, **27**(3), 114–128.
- 48 M. Klarhöfer, B. Csapo, C. Balassy, J. C. Szeles and E. Moser, High-resolution blood flow velocity measurements in the human finger, *Magn. Reson. Med.*, 2001, **45**(4), 716–719.
- 49 Y. Zhang, S. Y. C. Lee, Y. Zhang, D. Furst, J. Fitzgerald and A. Ozcan, Wide-field imaging of birefringent synovial fluid crystals using lens-free polarized microscopy for gout diagnosis, *Sci. Rep.*, 2016, **6**, 28793.
- 50 Y. K. Song, J. S. Park, J. K. Kim and C. K. Kim, HPLC Determination of Dexamethasone in Human Plasma, *J. Liq. Chromatogr. Relat. Technol.*, 2004, **27**(14), 2293–2306.
- 51 N. S. Abdelwahab, N. W. Ali, M. M. Zaki, S. M. Z. Sharkawi and M. M. Abdelkawy, Simultaneous Determination of Thalidomide and Dexamethasone in Rat Plasma by Validated HPLC and HPTLC With Pharmacokinetic Study, *J. Chromatogr. Sci.*, 2019, **57**(2), 130–138.
- 52 R. B. Friedrich, A. Ravello, L. C. Cichota, C. M. B. Rolim and R. C. R. Beck, Validation of a simple and rapid UV spectrophotometric method for dexamethasone assay in tablets, *Quim. Nova*, 2009, **32**, 1052–1054.
- 53 G. N. R. Devi, V. Prathyusha, K. Shanthakumari and S. A. Rahaman, Development and validation of uv-spectrophotometric method for the estimation of dexamethasone sodium phosphate in bulk and pharmaceutical dosage form, *Indo Am. J. Pharm. Res.*, 2013, **3**(7), 5055–5061.
- 54 N. Pargaonkar, Y. M. Lvov, N. Li, J. H. Steenekamp and M. M. de Villiers, Controlled release of dexamethasone from microcapsules produced by polyelectrolyte layer-by-layer nanoassembly, *Pharm. Res.*, 2005, **22**(5), 826–835.
- 55 S. S. Stewart, J. E. Roldan, Y. M. Lvov and D. K. Mills, Layer-by-Layer adsorption of biocompatible polyelectrolytes onto dexamethasone aggregates, *Conf. Proc. IEEE Eng. Med. Biol. Soc.*, 2006, **1**, 1474–1477.
- 56 G. B. Patil, K. P. Ramani, A. P. Pandey, M. P. More, P. O. Patil and P. K. Deshmukh, Fabrication of Layer-By-Layer Self-Assembled Drug Delivery Platform for Prednisolone, *Polym.-Plast. Technol. Eng.*, 2013, **52**(15), 1637–1644.

